Arabian Journal of Geosciences (2021) 14:2648
https://doi.org/10.1007/s12517-021-09080-1

ORIGINAL PAPER

Coulomb stress change before and after 24.01.2020 Sivrice (Elazığ) Earthquake (Mw = 6.8) on the East Anatolian Fault Zone

Hamdi Alkan[1] · Aydın Büyüksaraç[2] · Özcan Bektaş[3] · Ercan Işık[4]

Received: 20 October 2021 / Accepted: 20 November 2021

Abstract

The East Anatolian Fault Zone (EAFZ) with an average length of 500 km is one of the most seismically active regions of Turkey, and many major earthquakes have occurred along this fault zone. The earthquake of 24 January 2020 (Mw = 6.8) with the epicenter in Sivrice (Elazığ) occurred on the EAFZ and caused loss of life and property. This study was carried out to investigate the Coulomb stress changes before and after the Sivrice mainshock by using 89 earthquakes (M ≥ 4.5) with different depth ranges (7.5, 15, 22.5, 30 km) that occurred in the EAFZ between 1997 and 2020. Coulomb stress change maps were created using the Sivrice (Elazığ) mainshock and subsequent earthquakes. The maps showed that the stress continued in the northeast and southwest directions and caused a positive Coulomb stress change. According to the Conrad discontinuity depth calculation obtained from the thermal investigation covering the EAFZ and its immediate surroundings, a value of 21.2 km was obtained. While there was no stress increase at depths deeper than 20 km before the Sivrice mainshock, there was a stress increase up to 30 km after the mainshock. Rigidity of crustal structure is higher between segments 1 and 5 compared to segment 6 according to results of Curie Point Depth (CPD) on the EAFZ. This induced the positive Coulomb stress change along with the fault segments at the deeper depth levels. The high Coulomb stress values were especially observed around the Palu-Hazar Lake and Çelikhan-Gölbaşı segments. Therefore, these segments were defined as the earthquake hazard potential region.

Keywords Coulomb stress · Earthquake · East Anatolian Fault Zone · Curie depth

Introduction

Earthquakes provide valuable information in understanding current tectonic movements. For this reason, when the distribution of earthquakes in the ground and their development in time can be followed accurately, the current movements of the earth's crust and the geological process can be learned with sensitivity. If tectonic processes and stresses in fault zones are monitored, it becomes possible to predict the regions where earthquakes will be effective.

Turkey is located within the Alpine-Himalayan Mountain Range. Anatolian, which is between Eurasia Plate in the north and the African-Arabian Plates in the south, developed depending on the ongoing movements of these plates and the geotectonic evolution of the old and new Tethys Oceans located between these plates. The paleotectonic units in Turkey are limited to four units as Pontides, Anatolides, Taurides, and Edge Folds from north to south based on the evolution of mountain belts (Ketin 1966). An ocean between the Anatolide/Tauride platform and the Arabian Plate was called New Tethys before the late Cretaceous time (Şengör 1979). This ocean began to close in the late Cretaceous. In the middle Miocene, the Arabian Plate collided with the Eurasian Plate along the northern flank of the Bitlis Thrust Belt Zone. As a result of this impact, Eastern Anatolia was stuck in the north–south direction, and a neotectonic period started on the entire Anatolian Plate. All the young and

Responsible Editor: Longjun Dong

✉ Özcan Bektaş
obektas@cumhuriyet.edu.tr

[1] Department of Geophysical Engineering, Van Yüzüncü Yıl University, 65080 Van, Turkey

[2] Çan Vocational School, Çanakkale Onsekiz Mart University, 17400 Çanakkale, Turkey

[3] Department of Geophysical Engineering, Sivas Cumhuriyet University, 58140 Sivas, Turkey

[4] Civil Engineering Department, Bitlis Eren University, 13000 Bitlis, Turkey

Published online: 27 November 2021

active tectonic movements, fracture zones, active faults, and earthquake activity observed throughout Turkey in the present time are the products of the collision event that started on average 12 my ago and continues.

These plates formed after the continental collision and were represented within the framework of kinematic rules. The plate tectonics of Anatolian and its surroundings and the boundaries between these plates are shown in Fig. 1. Accordingly, the Arabian Plate, which is a part of the African Plate, moves north towards the Eurasian Plate and compresses Eastern Anatolian. The Anatolian Plate moves to the west with the ease brought about by the slip on the North Anatolian Fault Zone (NAFZ) and East Anatolian Fault Zone (EAFZ) with the effect of this compression (Şengör et al. 1985). Similarly, the Iranian Plate is displaced to the northeast, revealing the compression caused by the Arabian Plate. It can be seen that earthquake epicenters are associated with these active neotectonic and fracture zones, even at the regional level according to Fig. 2.

After the collision of the Eurasian-Arabian Plates, the Eastern Anatolian narrowed by an average of 40–60% in the north–south direction for the last 10 million years, and the earth's crust thickened and risen. The East Anatolian region was bounded by the NAFZ and the EAFZ in the west (Fig. 1). In this region and in the northern Caucasus, the north–south compressional movement was found to be 30 mm/year, and it was stated that 10–40% of the deformation here was related to earthquakes (Jackson and McKenzie 1988). A significant part of the deformation passes over the EAFZ, which forms the border of this region with the Anatolian Plate in the west. Compression formed intermountain depression basins, strike-slip faults, opening cracks, folded-thrusted areas, and plio-quaternary (2 my) volcanic eruptions in the region.

The EAFZ, which is one of the few active fault zones in Turkey with an average length of 500 km, starts from Karlıova (Muş) junction and extends to the Mediterranean Sea via Türkoğlu (Kahramanmaraş) junction and shows a left-sided movement (Fig. 3). It splits into three or four branches at the Türkoğlu junction. While the northern branches unite with the Hellenic-Cypriot arc, the southern branch extends towards the Dead Sea Fault Zone (DSFZ). A part of the movement between the Arabian Plate and the Anatolian Plate occurs in this fault zone (McKenzie 1972). The features of the complex tectonic relations between the EAFZ, the DSFZ, and the eastern extension of the Cyprus

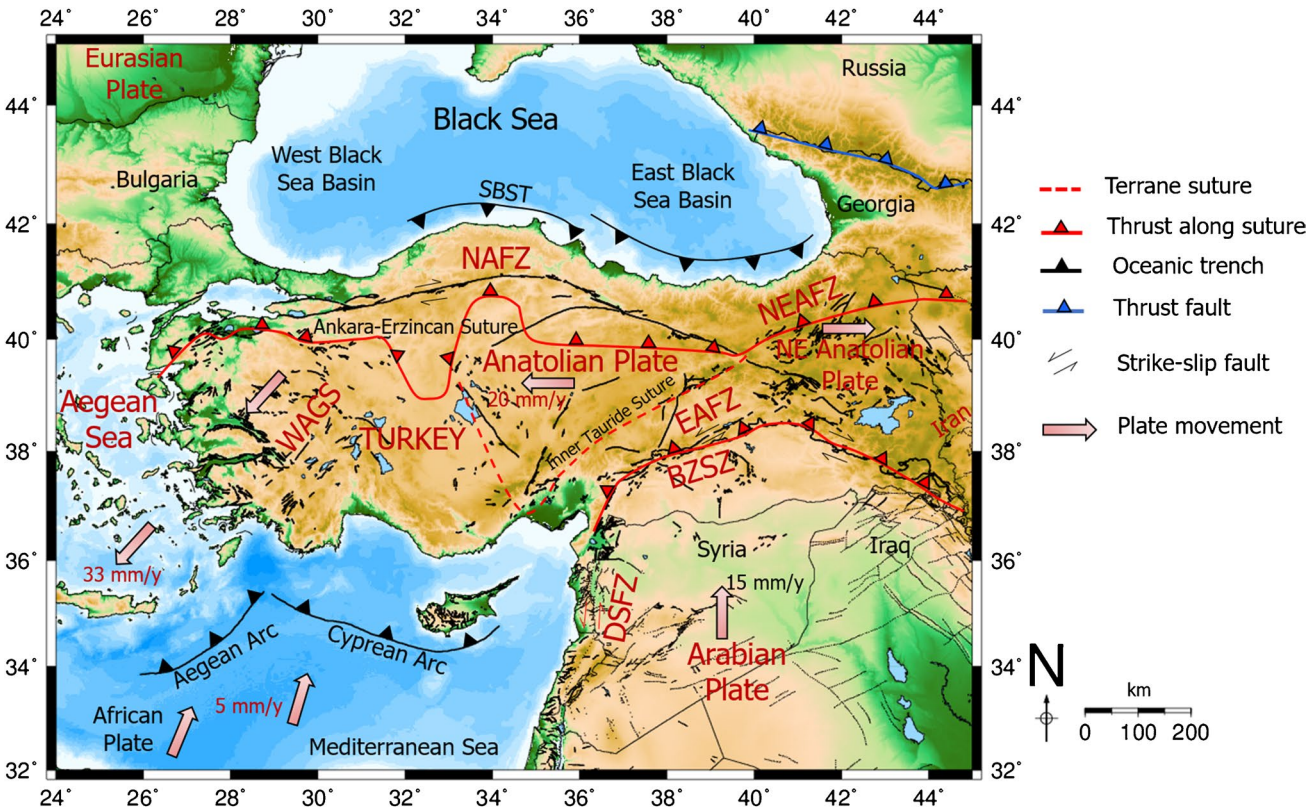

Fig. 1 Tectonic map of Turkey and the surrounding (modified from Işık et al. 2021 and Ekinci et al. 2020). NAFZ North Anatolian Fault Zone, EAFZ East Anatolian Fault Zone, NEAFZ Northeast Anatolian Fault Zone, BZSZ Bitlis-Zagros Suture Zone, DSFZ Dead Sea Fault Zone, WAGS West Anatolian Graben System, SBST Southern Black Sea Thrust

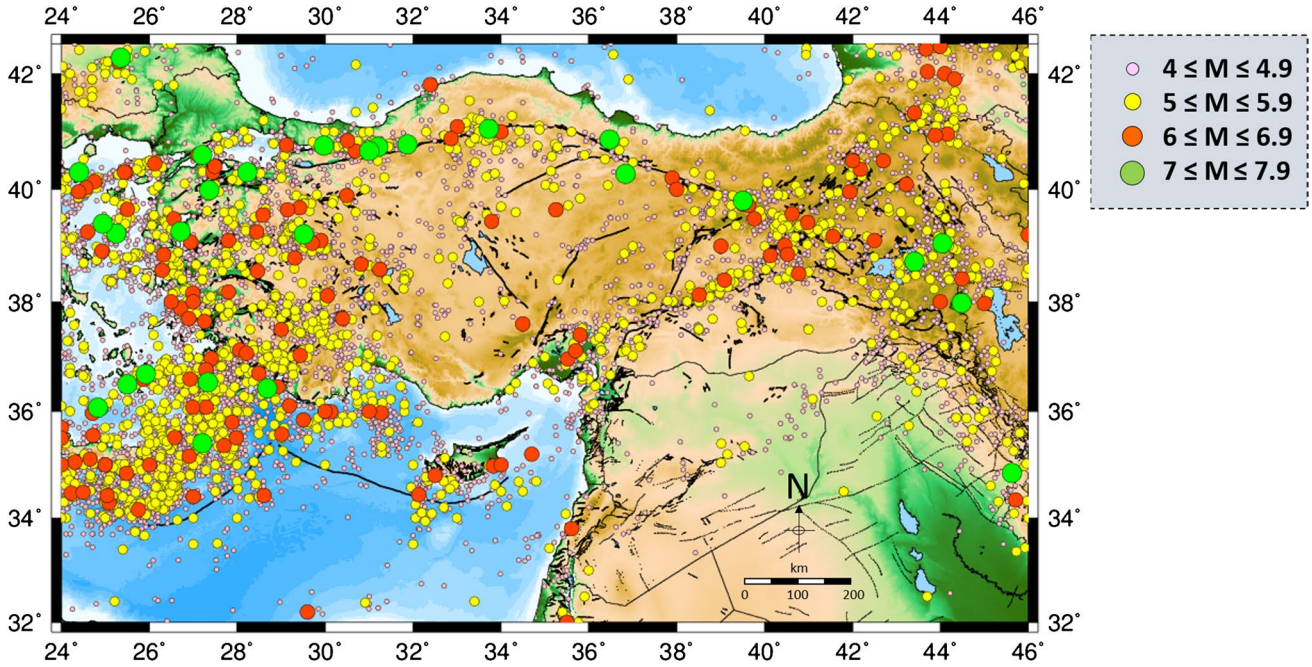

Fig. 2 Earthquakes with a magnitude greater than 4.0 between 1900 and 2021 in and around Turkey (Catalog information of earthquakes is taken from Kandilli Observatory and Earthquake Research Institute (http://www.koeri.boun.edu.tr/sismo/zeqdb/))

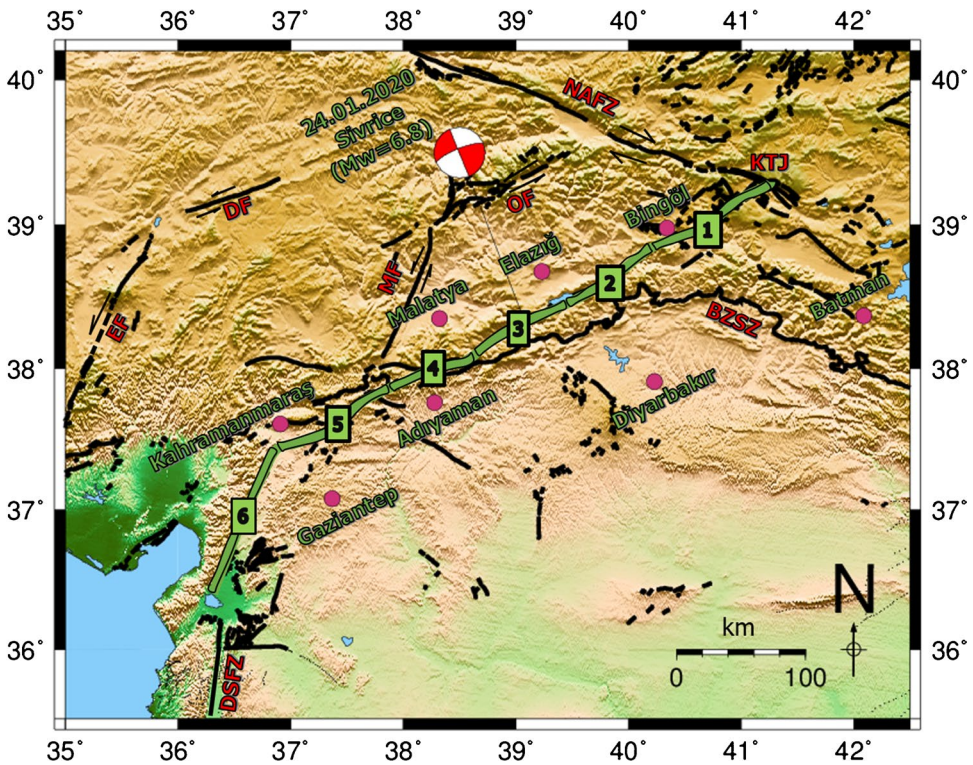

Fig. 3 The map depcits the fault segments of East Anatolian Fault Zone and the active faults around the EAFZ. (1:Karlıova-Bingöl, 2:Palu-Hazar Lake, 3:Hazar Lake-Sincik, 4:Çelikhan-Gölbaşı, 5:Gölbaşı-Türkoğlu, 6:Türkoğlu-Antakya. NAFZ North Anatolian fault zone, BZSZ Bitlis-Zagros suture zone, DSFZ Dead Sea fault zone, OF Ovacık fault, MF Malatya fault, DF Deliler fault, EF Erciyes fault) (modified from AFAD (2020) and Taymaz et al. 2021). The beach ball shows the focal mechanism of Elazığ (Sivrice) mainshock taken from AFAD (2020)

Arc remain as a problem that needs to be examined more. The kinematic features of the EAFZ are directly related to the movements on these two tectonic belts.

The effects of earthquakes occurring in a fault zone on the future can be examined by Coulomb stress analysis. The effects of previous earthquakes on the Gölcük (Kocaeli) (Mw = 7.4)

and Kaynaşlı (Düzce) (Mw = 7.2) earthquakes that occurred in Turkey in 1999 were examined using the Coulomb stress analysis, and it was understood that the Gölcük earthquake occurred in the region where the Coulomb stress increased due to previous events. The Kaynaşlı earthquake was triggered by the high increase in the static Coulomb stress transmitted by the Gölcük earthquake, despite the decrease in the stress on the Düzce Fault before 1999 (Çakır et al. 2003).

Analyses based on the Coulomb criterion were also carried out in the EAFZ. First, Nalbant et al. (2002) modeled 10 earthquakes and examined the increasing stress, and identified two fault segments. There is not an earthquake greater than 7.0 in the EAFZ since 1822. Destructive earthquakes occurred, but mostly due to the building quality in the region. Finally, Sünbül and Sünbül (2018) examined 18 earthquakes on the EAFZ and concluded that 12 of them were capable of creating interrelated stress transfer. In their study, they emphasized that the segment between Elazığ and Bingöl did not have a partial earthquake risk after the 2003 Bingöl and 2010 Elazığ earthquakes, whereas a stress increase was detected in the segment located between Kahramanmaraş and Malatya provinces due to both earthquake triggers and tectonic movements.

When an earthquake occurs, it changes the stress state of nearby faults. The Coulomb failure stress to estimate the stress state is calculated after Okada (1985) using elastic dislocations on rectangular planes in a homogeneous and isotropic semi-space. The accuracy of Coulomb stress changes resulting from an earthquake depends primarily on the accuracy of that earthquake's source parameters (i.e., the location and geometry of fault rupture and the amount and the feel of slip distribution). More accurate welding parameters, more reliable results, and therefore interpretations can be made.

The Sivrice (Elazığ) earthquake (Mw = 6.8) on the EAFZ on 24 January 2020 caused loss of life and property. The information was given about the seismotectonic setting and regional seismicity along EAFZ and also aftershock activity and ground motion data of this earthquake. Insufficient reinforcement and concrete strength, dimensions, and inadequate detailing increased the amount of damage in reinforced-concrete structures (Işık et al. 2020). The focal mechanism solution is consistent with pure left-lateral strike-slip faulting; the location of the epicenter and fault mechanism suggests deformation along the Pütürge segment of the EAFZ (Tatar et al. 2020).

Data and method

Coulomb stress changes

The displacement of a source fault or a dike causes static stress changes, and the displacement in the elastic halfspace is used to figure out the 3D strain field, multiplied by the elastic stiffness to derive the stress changes. The specified receiver faults, receiving stress from a mainshock, are planes with a specified strike, dip, and rake, on which the stresses imparted by the source faults are resolved. The shear stress change which depends on the position, geometry, and slip of the receiver fault including its rake, and the normal stress change which is independent of the receiver fault rake are taken into account to observe stress changes (Toda et al. 2011). The Coulomb stress change depends on the geometry and slip of the earthquake, the geometry and sense of slip of the fault, and the effective coefficient of friction (Stein et al. 1994). When the slip occurs on faults during an earthquake, the surrounding medium deforms, and its stress field changes (Ansari 2016). A measure of this change is calculated using the Coulomb failure criterion ($\Delta\sigma_{cfc}$). $\Delta\sigma_{cfc}$ can be expressed as

$$\Delta\sigma_{cfc} = \Delta\tau_s + \mu' \Delta\sigma_{n'} \quad (1)$$

Here, $\Delta\sigma_{cfc}$ is the change in failure stress on the receiver fault caused by slip on the source fault, $\Delta\tau_s$ is the change in shear stress (positive in the fault slip direction), $\Delta\sigma_{n'}$ is the change in normal stress (positive in extension), and μ' is the effective coefficient of friction on the fault (Toda et al. 2011). The effective coefficient of friction is dimensionless and varies between 0 and 1. In this study, it is considered as 0.4 in an elastic half-space with uniform isotropic elastic properties. For the source fault geometry, dimensionless Poisson's ratio is used as 0.25, and Young's modulus is chosen as 8×10^5 bars. The Coulomb stress changes between -0.1 and 0.1 (bar), in general, are enough to forecast upcoming future earthquakes (Yadav et al. 2012). The positive values of the Coulomb failure criterion reveal that stress is increasing, while the negative values of the Coulomb failure criterion indicate that stress is decreasing (Stein et al. 1994). The Coulomb stress variations are calculated using the Coulomb 3.3 software (Toda et al. 2011).

Data for Coulomb failure criterion

An earthquake slip causes stresses to change. The stress increases result in future earthquakes. Aftershocks are the most readily studied of such events because of their large number (King et al. 1994). To explain the time dependence of observed seismicity and distribution stress, it is necessary to choose a reasonable past seismicity time and mainshocks. On the other hand, the Coulomb stress changes are calculated for each large mainshock and the decay constant of aftershocks. Because the stress changes are substantially associated with the largest mainshock, the aftershocks do not fill in all stress-triggering lobes. However, the distributions of aftershocks expand into these positive lobes (King et al.

1994; Toda et al. 2005). Eighty-nine earthquakes (M ≥ 4.5) that occurred in the region between 1997 and 2020 were selected to investigate Coulomb stress transfer along with the East Anatolian Fault Zone (EAFZ). These earthquakes were processed separately as before and after the 24 January 2021 Elazığ-Sivrice mainshock (Mw = 6.8). The Coulomb stress changes were calculated for different depth levels (7.5, 15, 22.5, 30 km). Due to the lack of fault parameters in the reported earthquake catalogs, the time threshold time was chosen as 1997. The catalog information of events was published by AFAD and USGS and is listed in Table 1, consisting of date, latitude, longitude, magnitude, depth, strike, dip, and rake. Also, Fig. 4 shows the focal mechanisms and epicenter locations of all events and the 24 January 2021 Elazığ-Sivrice mainshock (Event No:24). According to Fig. 4, the focal mechanism results demonstrate generally strike-slip faults and thrust faults. Therefore, the stress changes have been resolved onto the optimally oriented strike-slip fault mechanism.

Results and discussion

The focal mechanism is an important feature of the seismic source, which has a major impact on the propagation of seismic waves (Ma et al. 2019). Even though the distance to the source is mostly the same, the dynamic conditions vary greatly in different directions (Ma et al. 2018, 2019). Therefore, it is necessary to understand the effects of the focal mechanism on the induced ground motions in the evaluation of seismic hazards. The EAFZ is one of the seismically most active regions in Turkey, and many large earthquakes occurred along this fault zone such as the 1966 Varto-Muş earthquake (Ms = 6.9), the 1971 Bingöl earthquake (Ms = 6.8), Kovancılar-Elazığ earthquake (Mw = 6.1) (AFAD 2020; Cheloni and Akıncı 2020). On 24 January 2020, the Elazığ-Sivrice mainshock (Mw = 6.8) caused widespread damage in the region, occurred in the Hazar Lake-Sincik segment of the EAFZ (Fig. 3). The focal mechanism solution of this last destructive earthquake was an ENE-WSW striking left-lateral strike-slip fault (AFAD 2020). These devastating earthquakes caused great changes in the seismicity rate, stress variations, and influence for seismic hazards referred to as earthquake interactions (Yazdanfar et al. 2018). In this paper, we investigate the Coulomb stress changes for two cases: (1) the Elazığ-Sivrice mainshock and subsequent events, (2) all events before the Elazığ-Sivrice mainshock.

All Coulomb stress computations are made for the depths of 7.5, 15, 22.5, and 30 km using a grid size of 0.1 by 0.1 km on the map view (Figs. 6 and 7). Increment and reduction in the stress variations are presented with red and blue colors, respectively. Also, the hypocenter distribution of selected earthquakes is depicted in Fig. 5 and is generally collected between 5 and 15 km. The number of earthquakes decreases rapidly at increasing depths. According to the Coulomb stress change maps, the Karlıova-Bingöl, Palu-Hazar Lake, and Hazar Lake-Sincik segments are partly stressed of all depth levels (Figs. 6 and 7). Conversely, in the Hazar Lake-Sincik segment, the stress value decreases at the depth of 15 km after the mainshock (Fig. 6). This may be due to the stress transfer of aftershock activity occurring at these depths (Fig. 5). The remarkable observation is that in the northeast of the EAFZ, around the Karlıova-Bingöl segment, there is total stress accumulation at the moderate depth. These high-stress values are due to the Karlıova triple junction that has thrust/reverse faults and strike-slip faults, Plio-Quaternary volcanic activity, crustal shortening, and a 2-km-high plateau (Alkan et al. 2020). On the other hand, we see that a slight stress increase has been observed at the depths of 22.5 km and 30 km in the northeast of the EAFZ due to the earlier earthquakes. Maden and Öztürk (2015) analyzed the relationships between the seismic *b*-values, Bouguer gravity, and heat flow data in the Eastern Anatolia region. The regional distribution of the *b*-value showed that the lower *b*-values (from 1.0 to 0.7) were observed in the EAFZ and the Bitlis Thrust Zone between 0 and 35-km depths. Laboratory studies on rock fractures show that a decrease in *b*-value is associated with higher shear stress and a reduction in restricted compression (Frohlich and Davis 1993). Also, When the *b*-value shows a decrease for a region, one can assess that there is a possibility of an earthquake occurrence in the next future (Öztürk 2017). In contrast to this, the variations of the Coulomb stress along the Çelikhan-Gölbaşı, Gölbaşı-Türkoğlu, Türkoğlu-Antakya segments are mostly low. The Gölbaşı-Türkoğlu and Türkoğlu-Antakya segments experienced a stress decrease at the shallow depth (Fig. 6), whereas they experienced positive stress change at the increasing depth (Fig. 7). Compared to other segments, the number of earthquakes occurring in these segments is quite low (Fig. 5). Therefore, we can identify these segments as slow seismic risks.

According to Coulomb stress change maps, the stress transfer continues in the direction of northeast and southwest (Figs. 6 and 7). There are four lobes with high-stress value, located in two lobes with NW–SE striking and two lobes with ENE-WSW striking. On the contrary, there are four lobes with low-stress value, located in two lobes with NE-SW striking and two lobes with NW–SE striking. It is an important note that the stress variation is positive in the Palu-Hazar Lake and Çelikhan-Gölbaşı segments for all depth levels. For each depth level, Karlıova-Bingöl and Gölbaşı-Türkoğlu segments have relatively lower and positive stress values. The aftershocks are mostly located in high-stress regions on optimally oriented strike-slip faults, and thus the aftershocks are most likely to be triggered

Table 1 Focal mechanism results for earthquakes occurring in the study area (36–39.5°N latitude and 35–42°E longitude). The focal mechanism results of earthquakes that occurred after 2007 are compiled from the AFAD website and the focal mechanism results of earthquakes that occurred before 2007 are compiled from the USGS website. (https://deprem.afad.gov.tr/faycozumleri?lang=en) (https://www.usgs.gov/natural-hazards/earthquake-hazards/earthquakes)

No	Date (dd mm yy)	Latitude (°N)	Longitude (°E)	Mag (Mw)	Depth (km)	Strike (°)	Dip (°)	Rake (°)
1	27/12/2020	38.521	39.181	5.3	15.94	211.0	41.0	−41.0
2	27/11/2020	38.208	38.606	4.7	6.94	325.0	76.0	−149.0
3	18/09/2020	38.705	38.094	4.5	7.01	349.0	82.0	171.0
4	16/09/2020	38.705	41.981	4.7	17.08	231.0	64.0	40.0
5	08/09/2020	38.180	38.688	4.6	11.42	245.0	81.0	−21.0
6	04/08/2020	38.238	38.762	4.8	3.90	329.0	80.0	174.0
7	04/08/2020	38.219	38.724	5.2	8.16	60.0	79.0	6.0
8	15/06/2020	39.367	40.743	5.6	7.01	271.0	82.0	174.0
9	14/06/2020	39.366	40.748	4.7	9.28	257.0	89.0	166.0
10	14/06/2020	39.362	40.739	4.6	7.32	356.0	78.0	4.0
11	14/06/2020	39.365	40.714	5.7	8.00	355.0	70.0	9.0
12	05/06/2020	38.257	38.745	5.0	6.98	344.0	88.0	−104.0
13	19/03/2020	38.372	39.104	5.0	7.39	165.0	84.0	172.0
14	29/02/2020	38.442	39.235	4.6	8.15	233.0	87.0	8.0
15	25/02/2020	38.329	38.769	4.9	14.29	245.0	43.0	−15.0
16	03/02/2020	38.398	39.154	4.5	7.18	240.0	85.0	22.0
17	31/01/2020	38.491	39.328	4.5	15.56	212.0	85.0	−14.0
18	25/01/2020	38.374	39.131	5.1	16.40	244.0	58.0	−7.0
19	25/01/2020	38.276	38.753	4.5	11.01	245.0	81.0	−21.0
20	24/01/2020	38.418	39.152	4.5	14.84	246.0	84.0	4.0
21	24/01/2020	38.267	38.708	4.6	11.22	340.0	70.0	−162.0
22	24/01/2020	38.369	39.031	4.6	13.01	240.0	79.0	5.0
23	24/01/2020	38.414	39.200	4.5	7.03	257.0	78.0	5.0
24	24/01/2020	38.359	39.063	6.8	8.06	248.0	76.0	1.0
25	27/12/2019	38.389	39.015	4.9	11.88	346.0	86.0	−139.0
26	29/05/2019	39.271	39.884	4.5	7.28	336.0	86.0	−160.0
27	15/04/2019	38.768	38.160	4.5	17.77	166.0	60.0	−158.0
28	04/04/2019	38.386	39.120	5.2	8.92	345.0	84.0	173.0
29	25/03/2019	38.769	38.166	4.5	10.72	242.0	86.0	−15.0
30	19/08/2018	37.377	36.385	4.8	10.53	332.0	82.0	−136.0
31	24/04/2018	37.583	38.503	5.1	9.79	113.0	87.0	−177.0
32	02/03/2017	37.595	38.486	5.5	9.76	321.0	84.0	178.0
33	10/06/2016	39.011	40.712	4.5	12.81	21.0	74.0	−33.0
34	09/12/2015	38.817	37.849	4.5	17.54	328.0	70.0	174.0
35	07/12/2015	39.286	40.190	4.5	9.75	220.0	75.0	−11.0
36	02/12/2015	39.261	40.217	5.3	10.66	309.0	87.0	−171.0
37	29/11/2015	38.838	37.824	5.0	17.45	67.0	88.0	6.0
38	29/07/2015	36.564	35.036	5.0	29.68	319.0	75.0	165.0
39	10/02/2015	36.012	35.960	4.6	23.68	30.0	42.0	139.0
40	08/01/2015	37.090	36.805	4.6	8.00	19.0	74.0	−11.0
41	09/06/2014	36.612	36.065	4.5	20.56	356.0	41.0	−99.0
42	14/02/2014	36.752	36.037	4.5	15.67	352.0	45.0	−111.0
43	17/09/2013	39.051	41.398	4.9	19.01	216.0	90.0	−3.0
44	16/09/2013	39.029	41.434	4.5	19.46	33.0	90.0	−7.0
45	08/01/2013	37.936	37.978	4.7	15.35	326.0	83.0	−175.0
46	13/11/2012	37.305	37.120	4.7	23.41	207.0	74.0	−7.0
47	16/10/2012	37.271	37.137	4.6	28.96	39.0	72.0	−18.0

Table 1 (continued)

No	Date (dd mm yy)	Latitude (°N)	Longitude (°E)	Mag (Mw)	Depth (km)	Strike (°)	Dip (°)	Rake (°)
48	16/10/2012	37.277	37.148	4.6	13.30	25.0	77.0	−24.0
49	19/09/2012	37.283	37.139	5.1	22.35	213.0	79.0	−21.0
50	16/09/2012	37.505	35.663	4.7	24.21	226.0	57.0	9.0
51	22/07/2012	37.574	36.370	5.0	4.56	336.0	65.0	−118.0
52	25/05/2012	38.152	38.587	4.8	12.22	341.0	85.0	−159.0
53	28/04/2012	38.517	40.741	4.6	22.47	256.0	80.0	41.0
54	04/04/2012	36.953	37.070	4.7	20.71	224.0	72.0	13.0
55	16/02/2012	38.632	37.399	4.6	14.63	318.0	44.0	104.0
56	22/11/2011	39.024	35.893	4.5	11.12	151.0	90.0	−177.0
57	23/06/2011	38.556	39.630	5.3	13.42	259.0	83.0	15.0
58	16/11/2010	37.370	36.389	4.7	21.22	204.0	36.0	−61.0
59	14/11/2010	36.605	35.987	5.1	24.17	144.0	42.0	−58.0
60	17/09/2010	38.109	39.020	4.8	20.16	34.0	77.0	2.0
61	24/03/2010	38.771	40.093	5.0	22.57	234.0	53.0	−2.0
62	08/03/2010	38.741	40.033	4.8	15.67	55.0	83.0	15.0
63	08/03/2010	38.745	40.034	5.0	11.75	227.0	68.0	−11.0
64	08/03/2010	38.751	40.041	5.6	15.15	323.0	82.0	−150.0
65	08/03/2010	38.766	40.071	5.8	5.01	54.0	86.0	−1.0
66	07/07/2009	38.254	38.740	5.0	12.47	200.0	38.0	−41.0
67	17/01/2009	37.166	36.306	4.6	7.52	245.0	66.0	46.0
68	25/08/2007	39.251	41.093	5.5	23.88	145.0	42.0	−140.0
69	14/04/2007	38.352	39.284	4.5	4.88	244.0	57.0	8.0
70	09/03/2007	39.063	40.470	4.8	5.00	238.0	85.0	2.0
71	08/03/2007	39.108	40.441	4.8	26.40	313.0	79.0	−152.0
72	28/02/2007	38.226	39.237	5.2	26.11	245.0	59.0	14.0
73	21/02/2007	38.382	39.308	5.4	8.51	262.0	60.0	6.0
74	02/07/2006	39.274	40.960	5.0	3.00	290.0	63.0	−163.0
75	10/12/2005	39.394	40.946	5.4	10.00	277.0	76.0	−177.0
76	26/11/2005	38.260	38.814	5.1	8.50	237.0	51.0	−20.0
77	06/06/2005	39.220	41.080	5.6	10.00	293.0	71.0	−167.0
78	23/03/2005	39.431	40.925	5.7	10.00	188.0	77.0	−13.0
79	14/03/2005	39.354	40.890	5.8	5.00	287.0	75.0	−165.0
80	12/03/2005	39.440	40.978	5.6	11.10	191.0	70.0	−15.0
81	11/08/2004	38.377	39.261	5.7	7.40	245.0	83.0	−4.0
82	13/07/2003	38.288	38.963	5.6	10.00	342.0	89.0	179.0
83	01/05/2003	39.007	40.464	6.4	10.00	333.0	67.0	−171.0
84	27/01/2003	39.500	39.878	6.1	10.00	62.0	88.0	−15.0
85	17/10/2002	39.443	40.275	4.8	10.00	308.0	36.0	156.0
86	25/06/2001	37.238	36.206	5.5	5.00	189.0	15.0	−83.0
87	06/04/1999	39.400	38.307	5.4	10.00	326.0	49.0	175.0
88	09/05/1998	38.780	38.988	5.1	10.00	341.0	83.0	−174.0
89	22/01/1997	36.250	35.951	5.7	10.00	243.0	39.0	−15.0

due to the Coulomb stress transfer (Çakır et al. 2003). Öztürk (2017; 2018) carried out the current earthquake potential in the Eastern Anatolia region using the seismotectonic *b*-value, seismicity rate changes Z-value, and fractal correlation dimension *Dc* value. A significant decrease in *b*-value (≤ 1.0), clear quiescence anomalies in *Z*-value, and high *Dc* value (≥ 2.2) were observed in the southeastern part of the EAFZ, and the junction of the Eastern Anatolia and DSFZ. These anomalies may be an indicator of stress increases and may show the quiescence regions before the next earthquake occurrences. According to the AFAD earthquake department, earthquakes that

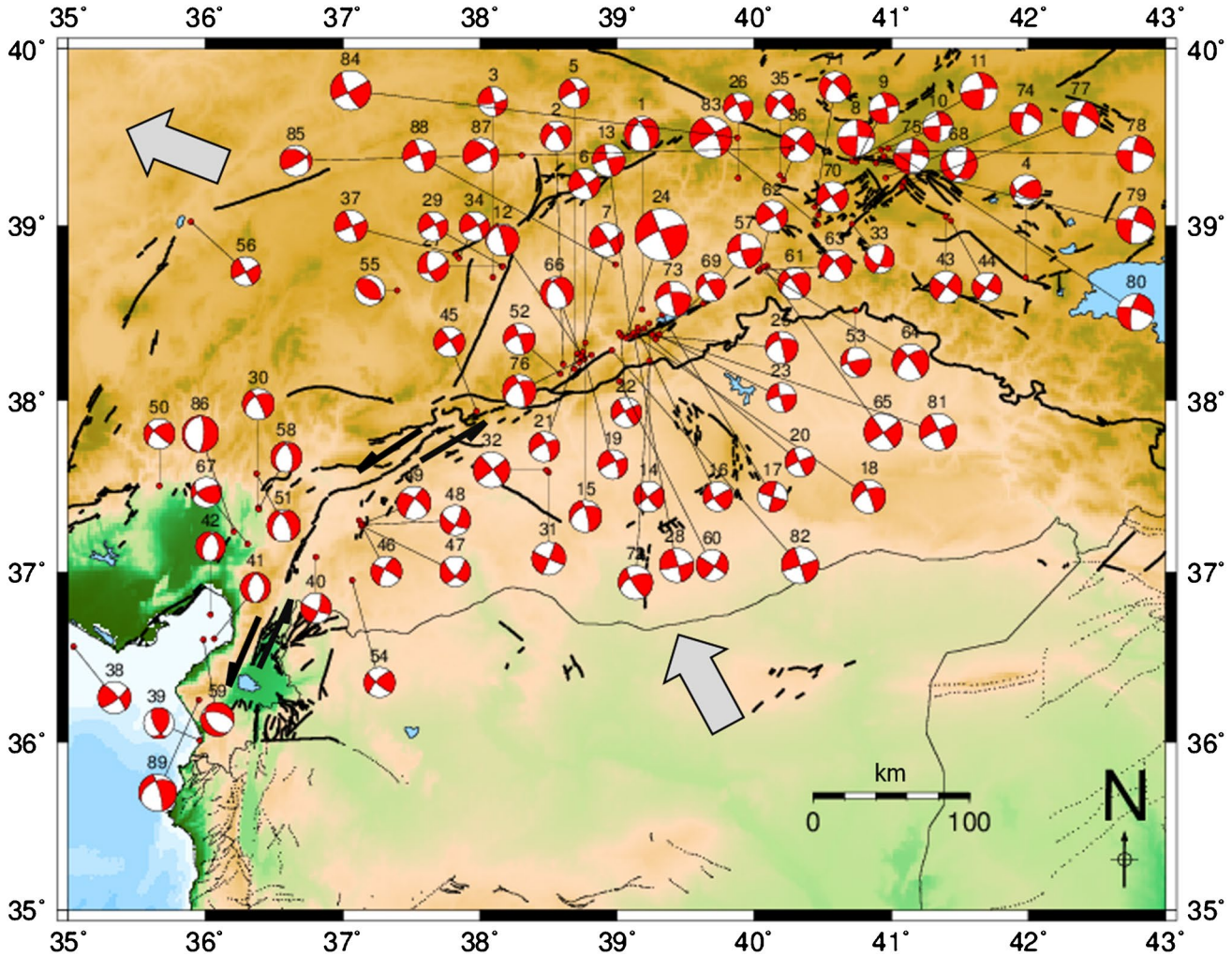

Fig. 4 Focal mechanism results from the events that occurred along the East Anatolian Fault Zone (See Table 1 for details). The active fault database is taken from Emre et al. (2018). The figure is prepared by using Generic Mapping Tools (GMT) (Wessel et al. 2013)

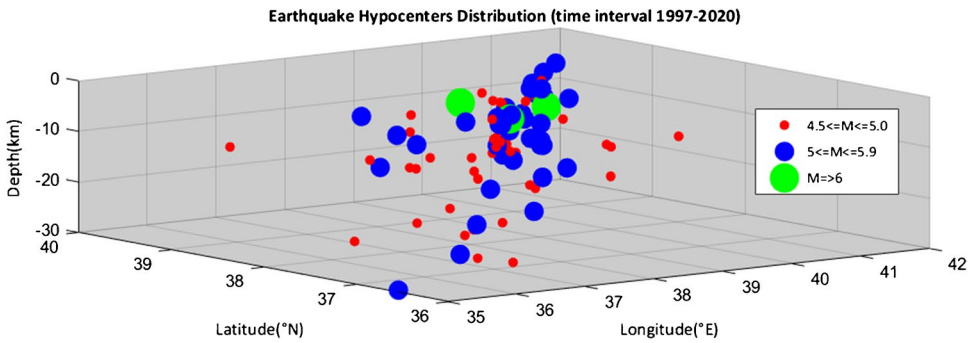

Fig. 5 The distribution of earthquake hypocenters occurred in 1997–2020. The catalog information of earthquakes was taken from the AFAD and USGS

occurred on 25 June 2021 in Bingöl (Kiğı) (Mw = 5.2) and 29 June 2021 in Elazığ (Maden) (Mw = 4.3) confirm high-stress values of the Palu-Hazar Lake and Çelikhan-Gölbaşı segments. Especially in the Hazar Lake-Sincik segment, high-stress values are striking in the 30-km depth map compared to other stress variations. This stress transfer may have resulted from the mainshock which was a shallow (depth = 8.6 km) event. However, high seismic activity is not observed around Adıyaman and Diyarbakır provinces (Fig. 5). Also, negative Coulomb stress is clearly observed around the Malatya fault located north of the EAFZ. In contrast, stress variation is positive in the

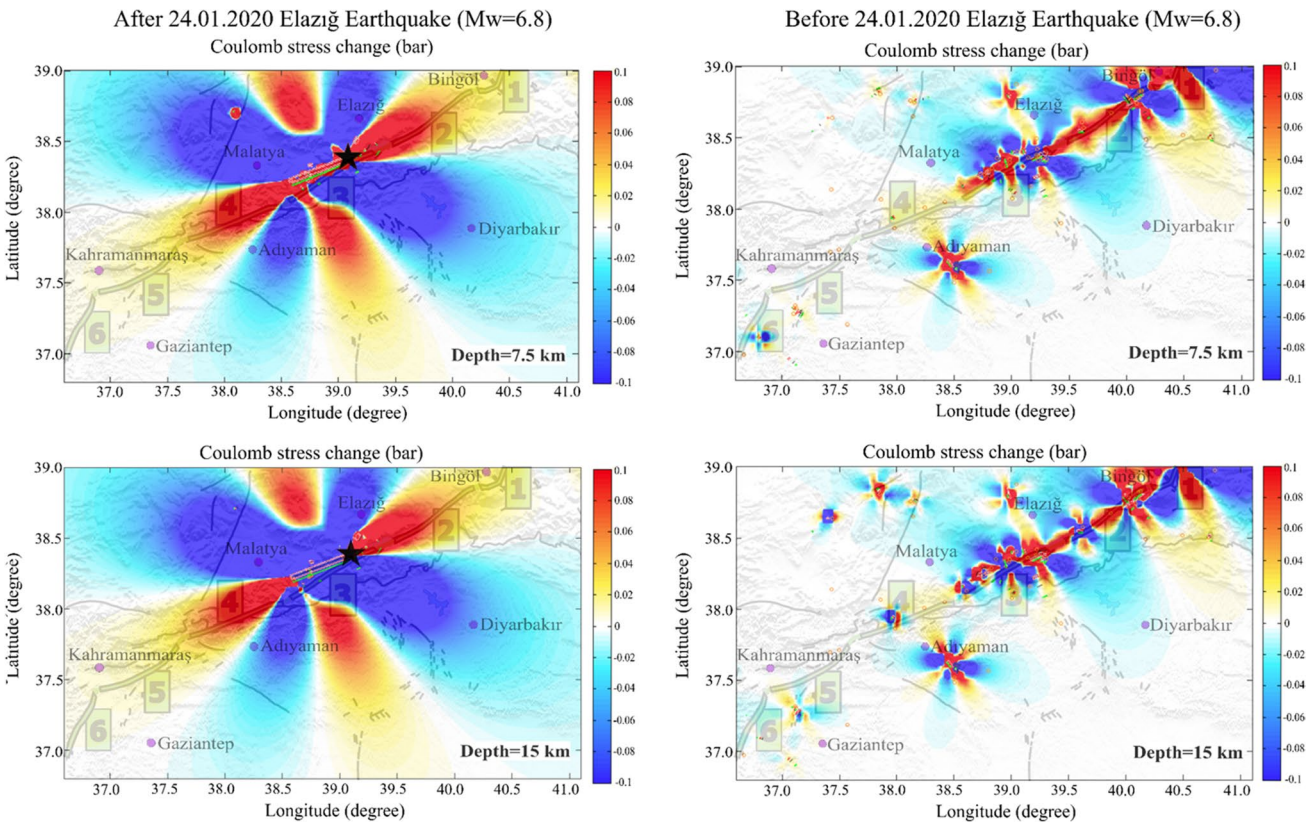

Fig. 6 Coulomb stress changes along the East Anatolian Fault Zone for the depths of 7.5 km and 15 km. (Left) The maps depict stress changes obtained from 24 January 2020 Elazığ-Sivrice mainshock (black star) and subsequent events. (Right) The maps depict stress changes obtained from the events before the 24 January 2020 Elazığ-Sivrice mainshock. The events catalog information is given in Table 1. The segments of the East Anatolian Fault System are modified from AFAD (2020). 1:Karlıova-Bingöl, 2:Palu-Hazar Lake, 3:Hazar Lake-Sincik, 4:Çelikhan-Gölbaşı, 5:Gölbaşı-Türkoğlu, 6:Türkoğlu-Antakya

north of Malatya fault connected with the Ovacık fault. Around the Türkoğlu-Antakya segment, connected with the Dead Sea fault zone, moderate stress values are generally observed. This region generally produced moderate or small earthquakes (Figs. 4 and 5).

An earthquake greater than 7.0 did not occur in the instrumental period. On the other hand, the earthquakes that occurred in the region made significant damage. The most important reason for these seismic events was low-quality constructed buildings. Adobe-stone masonry style is widely used along the EAFZ, especially in rural areas, and generally consists of 1–2 stories built by local craftsmen and workers using local materials without any engineering service. The earthquake performance of such structures is not sufficient, and therefore the number of damage increases. This reveals the importance of earthquake-resistant building design rules in regions with high seismic hazard. In this context, these rules in Turkey were updated in detail in 2018 and have been used since 2019.

Four main seismic crustal layers down to 40 km were determined by Özer et al. (2019) in the EAFZ. Conrad discontinuity was detectable at 20-km depth and seismogenic depth to vary from 0 to 20 km. Moho depth varied between 30 and 40 km according to Özer et al. (2019). On the contrary, the crustal thickness varied between 36 and 42 km according to Ateş et al. (2012) and Alkan (2021). Bektaş et. al. (2007) investigated Curie point depths by using aeromagnetic anomalies in Eastern Turkey. CPDs were calculated for 78 blocks with a size of 150×150 km^2. They determined that the Curie point depths of Eastern Anatolia varied from 12.9 to 22.6 km. In their study, heat flow values were obtained by using Lachenbruch and Sass (1978) model for B24, B25, B36, B37, B38, and B39 block numbers (Bektaş et al. 2007). In the calculation process of heat flow values, they assumed that thermal conductivity was 2.5 Wm^{-1} K^{-1} (k), the effective depth of heat production was 10 km (D), linear heat production was 2.09 μWm^{-3} (A_0), and horizontal strain rate was %0 (s). Calculated heat flow values for every 6 blocks are given in Table 2. Surface heat flow values (qs) vary between 83.9 and 111.9 mWm^{-2} in the study region. Depth values corresponding to 680 °C from the 1D geothermal gradient

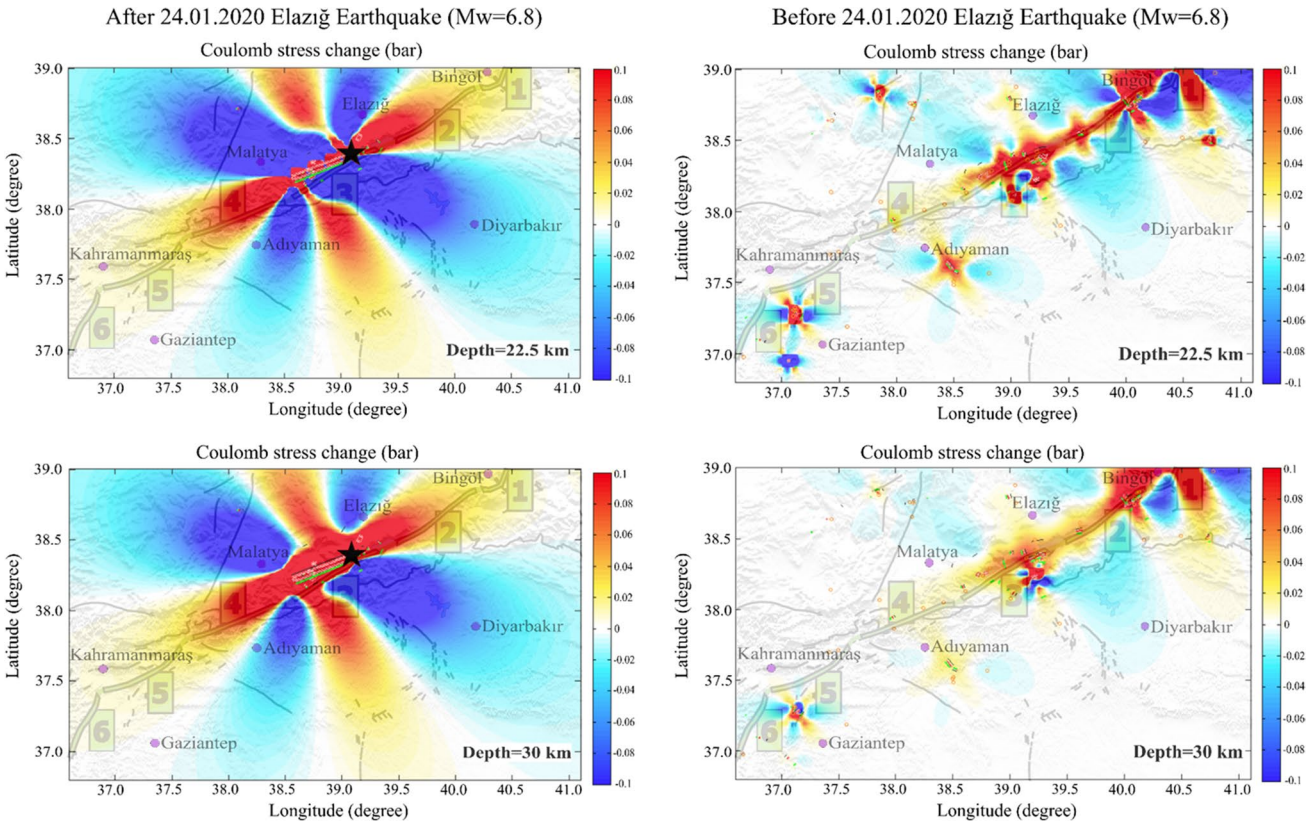

Fig. 7 The same as Fig. 6, but for depths of 22.5 km and 30 km

Table 2 Astenospheric heat flow (q_a), regional heat flow (q_r), surface heat flow (q_s), 580 °C depths for Lachenbruch and Sass (1978) of thermal models and Curie point depths (CPD) for 6 blocks B: Bektaş et. al. (2007), Turkey. LS: Lachenbruch and Sass (1978)

Block number	q_a (mW m^{-2})	q_r (mW m^{-2})	q_s (mW m^{-2})	Depth (km) (580°C) for *LS*	CPD (km) For *B*	Depth (km) (680°C)
B24	75	75	95.9	17.05	16.9	20.25
B25	79	79	99.9	16.23	16.3	19.26
B36	63	63	83.9	20.14	20.1	23.97
B37	71	71	91.9	17.97	17.9	21.35
B38	81	81	101.9	15.85	15.8	18.8
B39	65	65	85.9	19.55	19.4	23.25

changes obtained in the study region are shown in Table 2, and the average depth is determined as 21.1 km. Özer et al. (2019) suggested the Conrad discontinuity value as 20 km for the study region, and it was a good correlation with the average depth value at 680 °C.

Conclusions

Although the stress increase before the 24 January 2020 (Mw = 6.8) Sivrice (Elazığ) mainshock is partially observed in the Karlıova-Bingöl, Palu-Hazar Lake, and Hazar Lake-Sincik segments, the most significant stress increase is recorded in the Karlıova-Bingöl segment in the northeast of the EAFZ. In contrast, the Coulomb stress variations along the Çelikhan-Gölbaşı, Gölbaşı-Türkoğlu, Türkoğlu-Antakya segments are mostly low. While Gölbaşı-Türkoğlu and Türkoğlu-Antakya segments experience a stress reduction at shallow depth, a positive stress variation is observed at increasing depth. Therefore, changes in these segments are defined as a slow seismic hazard. According to the Coulomb stress variation maps created by using the Elazığ-Sivrice mainshock and subsequent earthquakes, there are four stress increase lobes in two lobes with N-S pulse and two lobes with EE-WSW pulse, and four-lobe stress reductions in two lobes with

NE-SW pulse and two lobes with E-W pulse. Stress variation is positive for all depth levels in Palu-Hazar Lake and Çelikhan-Gölbaşı segments. Karlıova-Bingöl and Gölbaşı-Türkoğlu segments have relatively lower but positive stress values for each depth level. Aftershocks were mostly located in regions of stress increase on optimally oriented strike-slip faults (Hazar Lake-Sincik, and Çelikhan-Gölbaşı fault segments). The 25 June 2021 Bingöl (Kiğı) (Mw = 5.2) and 29 June 2021 Elazığ (Maden) (Mw = 4.3) earthquakes confirm the increased stress values of these segments. Especially in the Hazar Lake-Sincik region, where the mainshock occurred, the 30-km depth map shows higher stress values compared to other stress maps. Since 24 January 2020, the Elazığ-Sivrice mainshock was shallow (depth = 8.6 km); stress may have been transferred to increasing depths. In addition, there is no seismic load in Diyarbakır and Adıyaman provinces located near the EAFZ. However, an increase in stress is observed in the region between the two provinces. In addition, negative Coulomb stress is clearly observed around the Malatya fault located in the north of the EAFZ, while the stress variation is positive in the north of this fault, which is related to the Ovacık fault. Around the Türkoğlu-Antakya segment, which is thought to be associated with the Dead Sea fault zone, medium stress values are generally observed in which this region has produced moderate or small earthquakes from past to present. Sivrice (Elazığ) mainshock caused positive Coulomb stress variation with fault segments at different depth levels. According to the Conrad discontinuity depth calculation obtained from the thermal investigation covering the EAFZ and its immediate surroundings, a value of 21.2 km was obtained. This value was previously reported by Özer et al. (2019), which agrees with the 20-km value obtained. The Curie point depth (CPD) is approximately constant and varies in the range of 17–19 km in segments 1, 2, and 3. In segment 4, the CPD deepens and reaches over 20 km. In segment 5, its width varies between 17 and 19 km. The CPD becomes quite shallow and varies in the range of about 13–17 km in segment 6. This change naturally shows a parallel change in the heat flow (HF). Except for segment 6, no HF is observed above 100 mWm^{-2}. In this case, it can be said that there is a more rigid crustal structure between segments 1 and 5 compared to segment 6. This situation is also compatible with Conrad discontinuity. In addition, the reason for the shallow focal depths of the earthquakes observed along the EAFZ can also be explained by this situation. While there was no increase in stress at depths deeper than 20 km before the Sivrice mainshock, there was an increase in stress up to 30 km after the earthquake. A similar situation is observed in NE of Kahramanmaraş, where the stress is transferred (point 25, Table 2). Subsequent earthquake effects should be expected between Elazığ and Bingöl, NE of Kahramanmaraş, and between Adıyaman and Diyarbakır.

Declarations

Competing interests The authors declare that they have no competing interests.

References

AFAD (2020) https://tdth.afad.gov.tr. (Accessed 15 May 2021)

Alkan H, Çınar H, Oreshin S (2020) Lake Van (Southeastern Turkey) experiment: receiver function analyses of lithospheric structure from teleseismic observations. Pure Appl Geophys 177:3891–3909. https://doi.org/10.1007/s00024-020-02447-7

Alkan H (2021) Crust and uppermost mantle velocity structure beneath the East Anatolian Fault Zone from joint ınversion of P-receiver functions and Rayleigh wave group velocities. Eur J Sci Tech 21:285–300. https://doi.org/10.31590/ejosat.818592

Ansari S (2016) Co-seismic stress transfer and magnitude-frequency distribution due to the 2012 Varzaqan-Ahar earthquake doublets (Mw 6.5 and 6.4), NW Iran. J Asian Earth Sci 132:129–137. https://doi.org/10.1016/j.jseaes.2016.10.006

Ateş A, Bilim F, Büyüksaraç A, Aydemir A, Bektaş Ö, Aslan Y (2012) Crustal structure of Turkey from aeromagnetic, gravity and deep seismic reflection data. Surv Geophys 33(5):869–885. https://doi.org/10.1007/s10712-012-9195-x

Bektaş O, Ravat D, Büyüksaraç A, Bilim F, Ateş A (2007) Regional geothermal characterization of East Anatolia from aeromagnetic, heat flow and gravity data. Pure Appl Geophys 164:975–998. https://doi.org/10.1007/s00024-007-0196-5

Cheloni D, Akıncı A (2020) Source modelling and strong ground motion simulations for the 24 January 2020, Mw 6.8 Elazığ earthquake. Turkey Geophys J Int 223:1054–1068. https://doi.org/10.1093/gji/ggaa350

Çakır Z, Barka AA, Evren E (2003) Coulomb stress interactions and the 1999 Marmara Earthquake sequence. Turkish Journal of Earth Sciences 12: 91–103. https://journals.tubitak.gov.tr/earth/issues/yer-03-12-1/yer-12-1-6-0301-5.pdf

Ekinci YL, Büyüksaraç A, Bektaş Ö, Ertekin C (2020) Geophysical investigation of Mount Nemrut stratovolcano (Bitlis, Eastern Turkey) through aeromagnetic anomaly analyses. Pure Appl Geophys 177:3243–3264. https://doi.org/10.1007/s00024-020-02432-0

Emre Ö, Duman TY, Özalp S, Şaroğlu F, Olgun Ş, Elmacı H, Çan T (2018) Active fault database of Turkey. Bull Earthquake Eng 16:3229–3275. https://doi.org/10.1007/s10518-016-0041-2

Frohlich C, Davis S (1993) Teleseismic b-values: Or, much ado about 1.0. J Geophys Res 98(B1):631–644

Işık E, Aydın MC, Büyüksaraç A (2020) 24 January 2020 Sivrice (Elazığ) earthquake damages and determination of earthquake parameters in the region. Earthq Struct 19(2):145–156. https://doi.org/10.12989/eas.2020.19.2.145

Işık E, Ekinci YL, Sayıl N, Büyüksaraç A, Aydın MC (2021) Time-dependent model for earthquake occurrence and effects of design spectra on structural performance: a case study from the North Anatolian Fault Zone, Turkey. Turkish J Earth Sci 30:215–234. https://doi.org/10.3906/yer-2004-20

Jackson J, McKenzie DP (1988) The relationship between plate motions and seismic moment tensors, and the rates of active deformation in the Mediterranean and Middle East. Geophys J 93:45–73. https://doi.org/10.1111/j.1365-246X.1988.tb01387.x

Ketin I (1966) Anadolu'nun tektonik birlikleri. Maden Tetkik Ve Arama Enst Derg 66:20–34

King GCP, Stein RS, Lin J (1994) Static stress changes and the triggering of earthquakes. Bull Seismol Soc Am 84(3):935–953

Lachenbruch AH, Sass JH (1978) Models of an extending lithosphere and heat flow in the basin and range province. In (Smith, R. B. and Eaton, G. P. eds.), Cenozoic Tectonics and Regional Geophysics of the Western Cordillera. Geol Soc Amer Mem 152: 209–250

Ma J, Dong L, Zhao G, Li X (2018) Discrimination of seismic sources in an underground mine using full waveform inversion. Int J Rock Mech Min Sci 106:213–222. https://doi.org/10.1016/j.ijrmms.2018.04.032

Ma J, Dong L, Zhao G, Li X (2019) Focal mechanism of mining-ınduced seismicity in fault zones: a case study of Yongshaba Mine in China. Rock Mech Rock Eng 52:3341–3352. https://doi.org/10.1007/s00603-019-01761-4

Maden N, Öztürk S (2015) Seismic b values, Bouguer gravity and heat flow data beneath Eastern Anatolia Turkey tectonic implications. Surv Geophys 36(4):549–570

McKenzie D (1972) Active tectonics of the Mediterranean region. Geophys J Roy Astron Soc. https://doi.org/10.1111/j.1365-246X.1972.tb02351.x

Nalbant SS, McCloskey J, Steacy S, Barka AA (2002) Stress accumulation and increased seismic risk in Eastern Turkey. Earth Planet Sci Lett 195(3–4):291–298. https://doi.org/10.1016/S0012-821X(01)00592-1

Okada Y (1985) Surface deformation due to shear and tensile faults in a half-space. Bull Seismol Soc Am 75(4):1135–1154. https://doi.org/10.1785/BSSA0750041135

Özer Ç, Özyazıcıoğlu M, Gök E, Polat O (2019) Imaging the crustal structure throughout the East Anatolian Fault Zone, Turkey, by local earthquake tomography. Pure Appl Geophys 176:2235–2261. https://doi.org/10.1007/s00024-018-2076-6

Öztürk S (2017) Space-time assessing of the earthquake potential in recent years in the Eastern Anatolia region of Turkey. Earth Sci Res J 21(2):67–75

Öztürk S (2018) Earthquake hazard potential in the Eastern Anatolian Region of Turkey: seismotectonic b and Dc-values and precursory quiescence Z-value. Front Earth Sci 12(1):215–236

Şengör AMC (1979) Mid-Mesozoic closure of Permo-Triassic Tethys and its implications. Nature 279:590–593

Şengör AMC, Gorur N, Saroglu F (1985) Strike-slip faulting and related basin formation in zones of tectonic escape: Turkey as a case study. Society of Economic Paleontologists and Mineralogists Special Publication 37: 227-264

Stein RS, King GCP, Lin J (1994) Stress triggering of the 1994 M = 6.7 Northridge, California, earthquake by its predecessors. Science 265(5177):1432–1435. https://doi.org/10.1126/science.265.5177.1432

Sünbül F, Sünbül AB (2018) Deprem Etkilesimlerinde Coulomb Gerilme Kriteri Degerlendirmesi; Dogu Anadolu Fay Hattı. Karaelmas Fen ve Müh Derg 8(2): 523-535. DOI: https://doi.org/10.7212/2Fzkufbd.v8i2.1166

Tatar O, Sozbilir H, Koçbulut F, Bozkurt E, Aksoy E, Eski S, Özmen B, Alan H, Metin Y (2020) Surface deformations of 24 January 2020 Sivrice (Elazığ)-Doğanyol (Malatya) earthquake (Mw=6.8) along the Pütürge segment of the East Anatolian Fault Zone and its comparison with Turkey's 100-year-surface ruptures. Med Geosc Rev 2(3):1–26. https://doi.org/10.1007/s42990-020-00037-2

Taymaz T, Ganas A, Yolsal-Cevikbilen S, Vera F, Eken T, Erman C, Keleş D, Kapetanidis V, Valkaniotis S, Karasante I, Tsironi V, Gaebler PJ, Melgar D, Öcalan T (2021) Source mechanism and rupture process of the 24 January 2020 Mw 6.7 Doğanyol–sivrice earthquake obtained from seismological waveform analysis and space geodetic observations on the East Anatolian Fault Zone (Turkey). Tectonophysics 804(3):228745. https://doi.org/10.1016/j.tecto.2021.228745

Toda S, Stein RS, Richards-Dinger K, Bozkurt SB (2005) Forecasting the evolution of seismicity in southern California: animations built on earthquake stress transfer. J Geophys Res 110:B05S16. https://doi.org/10.1029/2004JB003415

Toda S, Stein RS, Lin J (2011) Widespread seismicity excitation throughout central Japan following the 2011 M=9 0 Tohoku earthquake and its interpretation by Coulomb stress transfer. Geophys Res Lett Solid Earth 38:L00G03. https://doi.org/10.1029/2011GL047834

Wessel P, Smith WHF, Scharroo R, Luis JF, Wobbe F (2013) Generic mapping tools: improved version released. EOS Trans AGU 94:409–410. https://doi.org/10.1002/2013EO450001

Yadav RBS, Gahalaut VK, Chopra SB (2012) Tectonic implications and seismicity triggering during the 2008 Baluchistan, Pakistan earthquake sequence. J Asian Earth Sci 45:167–178. https://doi.org/10.1016/j.jseaes.2011.10.003

Yazdanfar C, Nemati M, Ataby MA, Roustaei M, Nilfouroushan F (2018) Stress transfer, aftershocks distribution and InSAR analysis of the 2005 Dahuieh earthquake, SE Iran. J Afr Earth Sc 147:211–219. https://doi.org/10.1016/j.jafrearsci.2018.06.022